https://doi.org/10.48048/tis.2025.9182

Silver Content Modification of Structural, Magnetic and Antibacterial Properties in Magnetite Nanoparticles

Fatimah Mufidza Zulhaina, Nurdiyantoro Putra Prasetya, Riyatun, Utari and Budi Purnama*

Department of Physics, Faculty of Mathematics and Natural Sciences, Universitas Sebelas Maret, Surakarta 57126, Indonesia

(*Corresponding author's e-mail: bpurnama@mipa.uns.ac.id)

Received: 21 October 2024, Revised: 2 December 2024, Accepted: 9 December 2024, Published: 20 January 2025

Abstract

The rising resistance of bacteria to traditional antibiotics has prompted the investigation of alternative antibacterial agents, including nanoparticles. Among these, silver-modified magnetite nanoparticles have attracted significant attention due to their unique properties and potential biomedical applications. In this study, silver (Ag) modified magnetite was synthesized to determine its antibacterial activity. Ag-modified magnetite nanoparticles with variation (x = 0, 0.02, 0.03 and 0.04) has been succesfully synthesied using the sol-gel method. X-ray diffractometer (XRD) results show that all peaks correspond to ICDD no 01-1111 owing face center cubic (fcc) with space groups Fd-3m. Calculation of crystallite size *D* using Schere's equation at the strongest peak shows an increase in the *D* with increasing x concentration from 23.22 to 35.28 nm. FTIR analysis indicates absorption peaks at 465 and 570 cm^{-1} which is typical original of magnetite absortion. Vibrating sample magnetometer, VSM result show that the magnetic saturation decrease with the increase of the x, i.e. 14.12 emu/g for x = 0 to 8.17 emu/g for x = 0.04. Finally, Ag-substituted magnetite nanoparticles show potential as antibacterial agents against *Eschericia coli* and *Staphylococcus aureus*, evidenced by the appearance of inhibition zones.

Keywords: Magnetite, Silver, Green synthesis, Antibacterial

Introduction

Nanotechnology has revolutionized various scientific fields by enabling the manipulation of materials at the nanoscale. Among these materials, nanoparticles have drawn significant attention due to their unique and enhanced properties compared to their bulk counterparts. Nanoparticles (NPs) are typically defined as solid particles with a size range of 10 - 1,000 nm, although the European Commission defines them as particles where at least half are equal to or smaller than 100 nm [1]. These particles exhibit distinctive electrical, optical, magnetic, biological and chemical properties, making them useful for a wide array of applications, including catalysis, energy storage, energy conversion and biomedical technologies [2-5].

In recent years, magnetite nanoparticles (Fe_3O_4) have gained prominence due to their superparamagnetic properties, biocompatibility and stability, making them ideal candidates for various applications such as drug delivery, magnetic resonance imaging (MRI) and hyperthermia treatments [6-9]. The ability to modify these nanoparticles further enhances their potential. One of the most promising modifications is doping or substituting magnetite with other elements to improve its functionality. Silver (Ag), for instance, has long been known for its excellent antibacterial properties [10-13]. This makes the addition of silver to magnetite nanoparticles potentially capable of producing materials that possess both magnetic properties and strong antibacterial activity [2].

The synthesis of magnetite substituted with silver nanoparticles (Ag/Fe_3O_4) aims to combine the advantageous properties of both materials. Ag nanoparticles are widely recognized for their broad-spectrum antibacterial effects, which have been

extensively studied in medical implants, wound dressings and coatings for medical devices [1,14]. The mechanism of silver's antibacterial action is primarily attributed to the release of Ag^+ ions, which can interact with bacterial cell membranes and DNA, causing cell death [6,15-17]. Meanwhile, magnetite's superparamagnetic behavior can be leveraged in targeted drug delivery and diagnostic applications, further enhancing the biomedical applications of the composite material [2].

One of the challenges in developing such composite materials is optimizing the synthesis process to achieve a homogenous distribution of silver within the magnetite matrix while maintaining the structural integrity of the magnetite nanoparticles. Various synthesis methods, including co-precipitation, sol-gel and hydrothermal techniques, have been explored to fabricate magnetite-silver composites. Since the sol-gel technique may be utilized for regulated size, shape and concentration of silver, it is crucial to choose it in conjunction with the green synthesis pathway [18-20]. Furthermore, the concentration of silver doping plays a crucial role in determining the material's overall properties, including its antibacterial efficacy and magnetic behavior. As studies have indicated, even small changes in silver concentration can significantly alter the characteristics of the material [2].

The aim of this research is to synthesize silver-substituted magnetite nanoparticles using green synthesis at varying concentrations and to investigate their structural, magnetic and antibacterial properties. The study focuses on providing a comprehensive understanding of how silver doping affects the magnetite matrix and exploring the potential of these composites as antibacterial agents. The findings from this research could contribute to the development of advanced materials with dual functionalities - magnetic and antibacterial - which have promising applications in medicine and biotechnology.

Experiment

The process begins with preparing the necessary equipment and materials. All tools and equipment are sterilized to ensure a contamination-free environment. After that, the required materials, including $Fe(NO_3)_3 \cdot 9H_2O$ (Merck) and $Ag(NO_3) \cdot 6H_2O$ (Merck), are carefully weighed for accuracy [$Fe(NO_3)_3 \cdot 9H_2O$: $Ag(NO_3) \cdot 6H_2O$ = 2 − x: x; x = 0, 2, 3, and 4 %]. Separate solutions of $Fe(NO_3)_3 \cdot 9H_2O$ (Merck) and $Ag(NO_3) \cdot 6H_2O$ (Merck) are prepared using deionized water as the solvent. The $Fe(NO_3)_3 \cdot 9H_2O$ (Merck) solution is then stirred for 5 min to ensure homogeneity. The Ag $(NO_3) \cdot 6H_2O$ (Merck) solution is gradually added to the $Fe(NO_3)_3 \cdot 9H_2O$ (Merck) solution. The mixture is stirred continuously for another 5 min to ensure proper incorporation of the 2 components. Lemon water (150 mL) is then added to the solution as a reducing agent, and the mixture is heated to 300 °C. It is crucial to maintain the temperature below 90 °C to avoid exceeding the threshold that might negatively impact the solution's properties. After heating, the solution starts to form a gel-like structure. This gel is stirred manually for 10 min, after which it is left to cool down to room temperature. The cooled gel undergoes a hydrolysis process at 100 °C for 24 h. This step is essential for further stabilizing the nanoparticle structure. After hydrolysis, the sample is ground for 1 h to achieve a finer particle size. The material is then annealed at 500 °C for 4 h. After annealing, the sample is subjected to an additional grinding process for 2 h to ensure uniformity in particle size. The final step, the treatment involved adjusting the Ag concentration (molarity = 0, 2, 3 and 4 %). The schematic synthesis process is shown in **Figure 1**. The synthesized nanoparticles are then characterized using various analytical techniques, including X-Ray Diffraction (XRD), Fourier-Transform Infrared Spectroscopy (FTIR), Vibrating-Sample Magnetometer (VSM) and antibacterial tests to assess their properties and potential applications. Finally, the collected data from the characterization tests are analyzed to draw conclusions about the material's structural, magnetic and antibacterial performance.

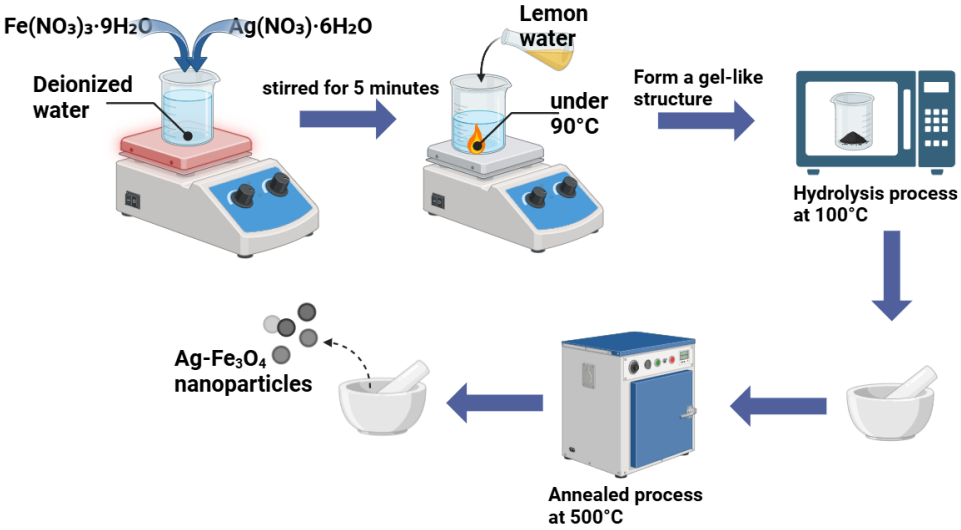

Figure 1 Schematic procedure of green synthesis for magnetite doping silver.

Results and discussion

Crystal structure analysis

The XRD pattern of silver-substituted magnetite (**Figure 2**) shows diffraction peaks at 2θ values around 30.09, 35.49, 43.09, 53.46, 56.98 and 62.60 °, corresponding to the (220), (311), (400), (422), (511) and (440) crystal planes of magnetite nanoparticles (MNP), consistent with JCPDS card 01-11111. The (311) plane is dominant, indicating a face-centered cubic (FCC) structure [21].

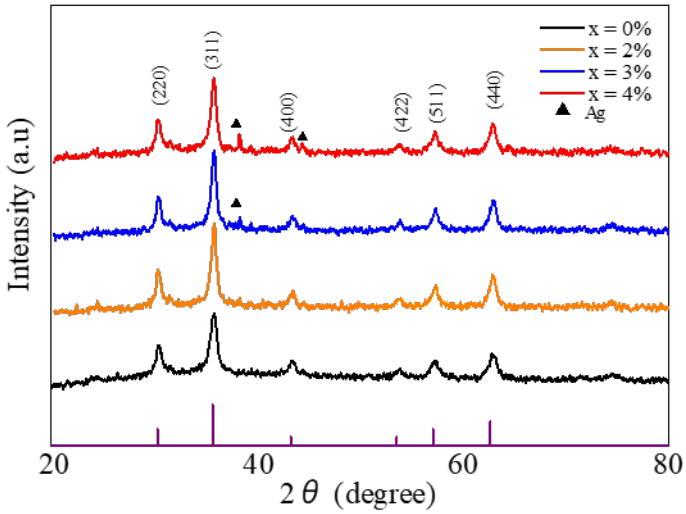

Figure 2 XRD pattern of green synthesis magnetite doping silver samples of doping variation (x = 0, 0.02, 0.03 and 0.04) annealing result of 500 °C for 4 h.

The peaks in the XRD pattern shown in **Figure 2** which are between 30 and 62 ° have corresponded to the standard magnetite [22]. All peaks match the International Center for Diffraction Data (ICDD) entry 01-1111 for FCC magnetite [23]. Ag doping at 2.00, 3.00 and 4.00 % increase α-phase peak intensities, suggesting an increase in crystallinity. However, at concentrations of 3 and 4 %, a new phase known as the Ag phase appeared, suggesting that the Ag ions in the magnetite nanoparticles were unable to completely replace the Fe ions. Calculation results for all XRD parameters (crystallite size, lattice parameters, lattice strain and density) are shown in **Table 1**.

$$D = k\lambda/\beta cos\theta \quad (1)$$

$$a = d\sqrt{h^2 + k^2 + l^2} \quad (2)$$

$$d_x = 8M/Na^3 \quad (3)$$

$$\varepsilon = \beta/4tan\theta \quad (4)$$

where, k represents a constant value of 0.94, λ denotes the wavelength of radiation (1.54054 Å for Cu Kα radiation), β refers to the full width at half maximum (FWHM) intensity of the peak, θ indicates the angle of diffraction, d is the spacing between crystal planes, (h, k and l) are the Miller indices corresponding to the (311) plane, M is the molecular weight and N represents Avogadro's number [24,25].

Higher Ag concentrations cause more pronounced peak shifts, especially in the (311) plane, confirming changes in lattice spacing and crystallinity. These structural modifications are likely to influence the material's antibacterial properties, warranting further investigation into their functional impact.

Table 1 Crystallite size, mean grain size, lattice strain, density of green synthesis magnetite doping silver samples of doping variation.

Doping	Crystallite size, *D* (nm)	Lattice parameter, *a* (Å)	Lattice strain, ε (10^{-3})	Density, d_x (g/cm^3)
0	23.22	8.3713	4.89	5.2421
0.02	25.60	8.3714	4.44	5.2419
0.03	32.52	8.3715	3.49	5.2417
0.04	53.28	8.3776	3.22	5.2303

Oxide group analysis

Fourier-transform infrared (FTIR) spectroscopy was employed to identify the functional groups adsorbed on the surface of silver-doped magnetite nanoparticles synthesized via the sol-gel method. The FTIR spectra for samples doped with 0.02, 0.03 and 0.04 mol % Ag, annealed at 500 °C for 4 h, exhibited 2 prominent absorption bands indicative of a cubic spinel structure. These bands correspond to the stretching vibrations of the Fe-O-Fe bond, which appear in the 300 - 600 cm^{-1} range, confirming the formation of magnetite [26].

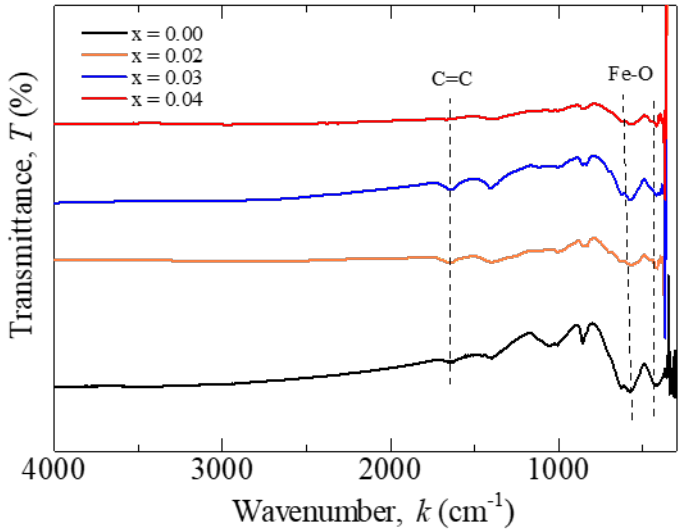

Figure 3 FTIR pattern of green synthesis magnetite doping silver samples of doping variation (x = 0, 0.02, 0.03 and 0.04) annealing result of 500 °C for 4 h.

The absorption peaks at approximately 570 cm^{-1} result from the splitting of the ν_1 band, observed at 570 and 416 cm^{-1}, likely due to the shifting of the ν_2 band, which corresponds to the Fe-O bond in bulk magnetite. This further verifies the presence of Fe_3O_4 in the synthesized nanoparticles. The v_1 band was positioned higher than the v_2 band, indicating shorter Fe-O bonds in the tetrahedral sites compared to the octahedral ones [27]. In addition, another absorption peak was observed at a wavenumber of approximately 1,600 cm^{-1}, indicating the presence of C=C bonds. This absorption suggests that the annealing process did not fully eliminate all impurities resulting from incomplete combustion during the synthesis. The force constant for Fe-O stretching remained consistent across different doping concentrations, while the force constant for Fe-O bending showed a decreasing trend with increasing silver doping concentration. The peaks observed at around 570 and 416 cm^{-1} in the Fe_3O_4 nanoparticles indicate the successful formation of magnetite. These findings were supported by the presence of Fe-O stretching bands, likely enhanced by the use of lemon extract during synthesis [21].

This result highlights the influence of silver doping on the structural properties of magnetite nanoparticles and the stability of Fe-O bonds within the cubic spinel framework. Subsequently, **Table 2** presents the results of the calculations for the force constants at the tetrahedral site (Eq. (5)) and the octahedral site (Eq. (6)) of the silver-modified magnetite nanoparticles.

$$k_{\mathrm{t}} = 7.62 M_1 k_1^2 \times 10^{-7} \frac{\mathrm{N}}{\mathrm{m}} \quad (5)$$

$$k_{\mathrm{o}} = 10.62 (\tfrac{M_2}{2}) k_2^2 \times 10^{-7} \frac{\mathrm{N}}{\mathrm{m}} \quad (6)$$

M_1 and M_2 represent the molecular weights of the cations located at the tetrahedral and octahedral sites, respectively [28].

Table 2 FTIR parameters of green synthesis magnetite doping silver samples of doping variation.

Doping	v_1 (cm^{-1})	v_2 (cm^{-1})	k_t (N/m)	k_o (N/m)	F (N/m)
0	576.74	416.64	14.15	5.15	8.15
0.02	569.99	374.21	13.83	8.53	11.18
0.03	570.95	364.56	13.87	8.10	10.99
0.04	570.95	366.49	13.87	8.19	11.03

Magnetic properties analysis

The magnetic properties of silver-doped magnetite synthesized via green synthesis were analyzed using Vibrating Sample Magnetometry (VSM), with an external magnetic field applied from −10 to 10 kOe. Hysteresis loops for iron sand samples doped with 0.02, 0.03 and 0.04 % Ag, annealed for 4 h, are shown in **Figure 4**, where the X-axis represents the external magnetic field (H) and the y-axis indicates magnetization (M).

As seen in **Figure 4**, the hysteresis loops widen and narrow with increasing Ag doping. The undoped magnetite sample shows a distinct hysteresis loop compared to the doped samples. All samples exhibit remanent magnetization (Mr) after the external field is removed, confirming their ferromagnetic properties. Key magnetic parameters, including coercivity (Hc), saturation magnetization (Ms) and remanent magnetization (Mr), are summarized in **Table 3**. Additionally, the coercive field and saturation magnetization can be utilized to assess magnetic anisotropy (K_a), as demonstrated in **Table 3** using the following equation [25],

$$K_a = \frac{Hc \times Ms}{0.96} \quad (7)$$

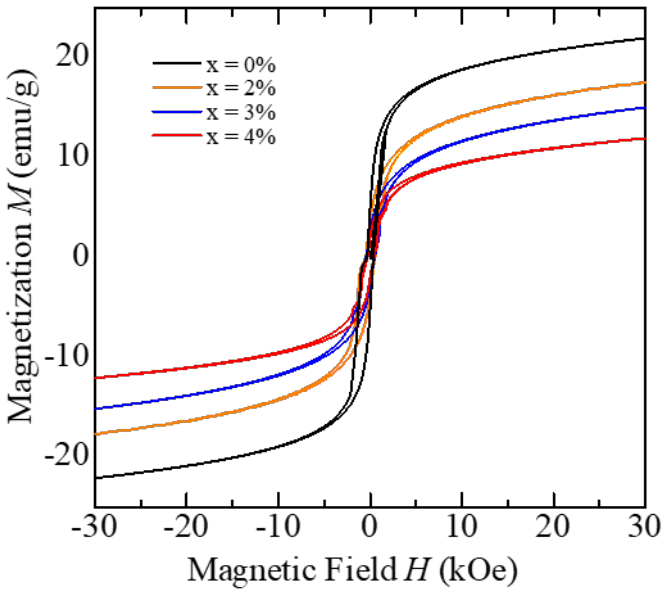

Figure 4 VSM Pattern of green synthesis magnetite doping silver samples of doping variation (x = 0, 0.02, 0.03 and 0.04) annealing result of 500 °C for 4 h.

Table 3 Parameter VSM of green synthesis magnetite doping silver samples of doping variation (x = 0, 0.02, 0.03 and 0.04) annealing result of 500 °C for 4 h.

Doping	H_C (Oe)	M_S (emu/g)	M_R (emu/g)	M_R/M_S	K_a (×10^3) (erg/cm^3)
0	330.71	14.12	5.42	0.38	4.86
0.02	498.21	11.72	3.81	0.32	6.08
0.03	483.43	9.06	3.04	0.31	4.86
0.04	426.67	8.17	2.35	0.29	3.63

The undoped sample shows a coercivity of 330.17 Oe, increasing to 498.21 Oe with doping, before decreasing to 426.67 Oe at higher doping levels. This change is attributed to domain wall pinning during domain nucleation, as described by Cullity and Graham [29]. According to Jiles [30], this coercivity variation depends on defect density and domain wall flexibility. Both saturation and remanent magnetization decrease with increasing Ag doping, likely due to the substitution of Fe^{3+}ions by Ag ions at octahedral sites, as noted by Ashraf *et al.* [31].

Antibacterial activity analysis

The antibacterial test results of silver-doped magnetite nanoparticles against *Escherichia coli* with varying doping concentrations (x = 0, 0.02, 0.03 and 0.04) showed inhibition zones ranging from 23.70 to 28.30 mm after 24 h of incubation. Meanwhile, the antibacterial test against *Staphylococcus aureus* showed inhibition zones ranging from 18.42 to 20.48 mm. This indicates significant antibacterial activity, where the nanoparticles interact with the bacterial cell wall, damage the membrane, and trigger the formation of reactive oxygen species (ROS) that cause bacterial cell damage [32,33]. The percentage of the area of the zone of inhabitation (ZOI) is determined by utilizing Eq. (8) [3].

$$\text{ZOI percentage (\%)} = \frac{\text{Surface area of ZOI (mm)}^2}{\text{Surface area of ZOI standard}^2} \times 100 \quad (8)$$

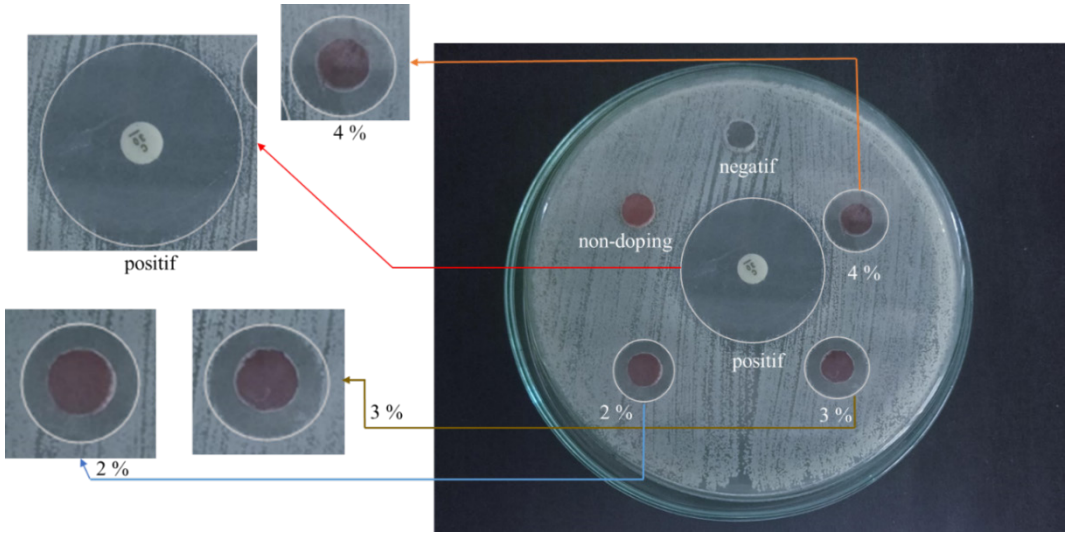

Figure 5 Antibacterial activity of green synthesis magnetite doping silver samples with concentration variations against *Stapylococcus aureus* bacteria.

Table 4 Magnetite doping silver inhibitory zone variation in concentration against *Stapylococcus aureus*.

Doping	***Staphylococcus aureus* (mm)**	**ZOI percentage (%)**
Positive	27.94	-
Negative	0	-
0	0	-
0.02	18.42	65.90
0.03	19.49	69.76
0.04	20.48	73.30

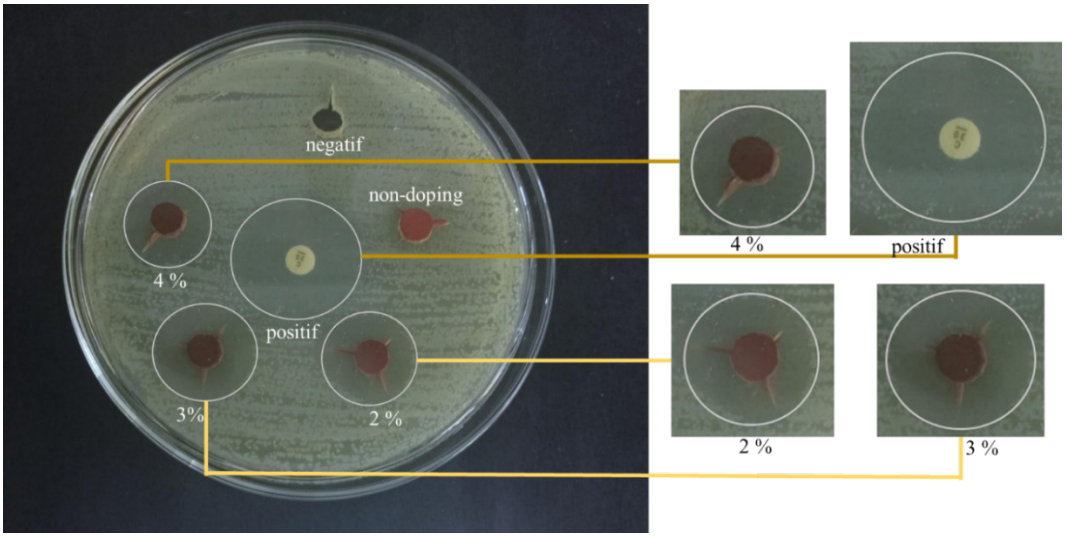

Figure 6 Antibacterial activity of magnetite doping silver samples with varying concentrations against *Escherichia coli* bacteria.

Table 5 Magnetite doping silver inhibitory zone variation in concentration against *Escherichia coli*.

Doping	*Escherichia coli* (mm)	ZOI percentage (%)
Positive	35.1	-
Negative	0	-
0	0	-
0.02	26.50	75.49
0.03	28.30	80.63
0.04	23.70	67.52

The difference in membrane structure between gram-positive and gram-negative bacteria affects their sensitivity to nanoparticles. Gram-positive bacteria, such as *S. aureus*, have thicker cell walls but are more sensitive to nanoparticles compared to the gram-negative *E. coli*, which has 2 membrane layers. ROS, generated by the reaction of Fe^{2+} ions, play a role in damaging bacterial cells and inhibiting their growth [34].

Overall, silver-doped magnetite nanoparticles show great potential as antibacterial agents, particularly against gram-negative bacteria such as *E. coli*. The results obtained from Ag-modified magnetite play an important role for future biomedical applications, one of which is in the development of targeted anticancer drug delivery systems [35].

Conclusions

The modification of magnetite nanoparticles with silver using green synthesis has been successfully carried out. The synthesis of silver-modified magnetite nanoparticles resulted in a cubic structure, confirmed by XRD data (ICDD 01-1111) with a face-centered cubic (fcc) unit cell. Increasing silver doping shifted the (311) hkl peak to higher angles, reducing the lattice constant and increasing the crystallite size from 23.22 to 35.28 nm. FTIR spectra confirmed the presence of Fe-O bonds typical of magnetite's spinel structure. Magnetically, the nanoparticles exhibited ferromagnetism, though both saturation and remanent magnetization decreased with higher silver doping. The nanoparticles showed promising antibacterial activity, with the highest silver doping enhancing efficacy against *E. coli* and *S. aureus*. Silver-doped magnetite nanoparticles are promising multifunctional materials with tunable magnetic and antibacterial properties, useful for biomedical applications such as antibacterial agents and magnetically guided drug delivery systems.

Acknowledgements

This research was funded by Penelitian Hibah Grup Riset Universitas Sebelas Maret, Indonesia contract number: 194.2/UN27.22/PT.01.03/2024.

References

[1] A Włodarczyk, S Gorgoń, A Radoń and K Bajdak-Rusinek. Magnetite nanoparticles in magnetic hyperthermia and cancer therapies: Challenges and perspectives. *Nanomaterials* 2022; **12(11)**, 1807.

[2] AAH El-Bassuony, WM Gamal and HK Abdelsalam. Impact of different magnetic materials added to silver-magnetite nanoparticles on the structural, magnetic and antimicrobial properties. *The European Physical Journal Special Topics* 2023; **232(8)**, 1339-1351.

[3] T Kusumaningsih, A Supriyanto, HB Akmal, FM Zulhaina, NP Prasetya and B Purnama. Nanoparticle-preparation-procedure tune of physical, antibacterial, and photocatalyst properties on silver substituted cobalt ferrite. *Results in Engineering* 2023; **18**, 101085.

[4] S Nayak, SS Nayak, AA Kittur, S Nayak and DR Joshi. Synthesis, fabrication, and performance evaluation of lanthanum doped nickel cobalt ferrite electrode for supercapacitors in energy storage applications. *Journal of Energy Storage* 2024; **101**, 113918.

[5] KO Abdulwahab, MM Khan and JR Jennings. Ferrites and ferrite-based composites for energy conversion and storage applications. *Critical Reviews in Solid State and Materials Sciences* 2024; **49(5)**, 807-855.

[6] Z Yang, H Sun, M Kurbonova, L Zhou, SG Arhin, VG Papadakis, MA Goula, G Liu, Y Zhang and W Wang. Simultaneous supplementation of magnetite and polyurethane foam carrier can reach a Pareto-optimal point to alleviate ammonia inhibition during anaerobic digestion. *Renewable Energy* 2022; **189**, 104-116.

[7] J Kurczewska and B Dobosz. Recent progress and challenges regarding magnetite-based nanoparticles for targeted drug delivery. *Applied Sciences* 2024; **14(3)**, 1132.

[8] S Zhang, Z Deng, B Yao, J Wu, Z Jiao and N Gu. Polyhedral magnetic nanoparticles of high magnetization synthesized by hydrocooling and magnetically internal heating coprecipitation: Implications for magnetic resonance imaging. *ACS Applied Nano Materials* 2024; **7(9)**, 10377-10386.

[9] JU Hassan, S Shahzadi, F Waheed, S Nawaz, R Sharif, S Riaz and D Ban. Synthesis, characterization, and biocompatibility of pure and doped magnetite nanoparticles for magnetic hyperthermia in cancer treatment. *Applied Physics A* 2024; **130(9)**, 635.

[10] S Wang, Y Zhang, X Chen, S Mourdikoudis, S Fan, H Li and G Zheng. Disentangling the "tip-effects" enhanced antibacterial mechanism of Ag nanoparticles. *Dalton Transactions* 2024; **53(29)**, 12281-12290.

[11] S Zhou, H Peng, A Zhao, R Zhang, T Li, X Yang and D Lin. Synthesis of bacterial cellulose nanofibers/Ag nanoparticles: Structure, characterization and antibacterial activity. *International Journal of Biological Macromolecules* 2024; **259**, 129392.

[12] G Vasiliev, AL Kubo, H Vija, A Kahru, D Bondar, Y Karpichev and O Bondarenko. Synergistic antibacterial effect of copper and silver nanoparticles and their mechanism of action. *Scientific Reports* 2023; **13(1)**, 9202.

[13] B Mohapatra, S Mohapatra and N Sharma. Biosynthesized Ag-ZnO nanohybrids exhibit strong antibacterial activity by inducing oxidative stress. *Ceramics International* 2023; **49(12)**, 20218- 20233.

[14] H Shao, T Zhang, Y Gong and Y He. Silver-containing biomaterials for biomedical hard tissue implants. *Advanced Healthcare Materials* 2023; **12(26)**, 2300932.

[15] H Li and H Xu. Mechanisms of bacterial resistance to environmental silver and antimicrobial strategies for silver: A review. *Environmental Research* 2024; **248**, 118313.

[16] A Hamad, KS Khashan and A Hadi. Silver nanoparticles and silver ions as potential antibacterial agents. *Journal of Inorganic and Organometallic Polymers and Materials* 2020; **30(12)**, 4811-4828.

[17] B Ekram, E Tolba, AF El-Sayed, WE Müller, HC Schröder, X Wang and BM Abdel-Hady. Cell migration, DNA fragmentation and antibacterial properties of novel silver doped calcium polyphosphate nanoparticles. *Scientific Reports* 2024; **14(1)**, 565.

[18] AG Niculescu, C Chircov and AM Grumezescu. Magnetite nanoparticles: Synthesis methods - a comparative review. *Methods* 2022; **199**, 16-27.

[19] LS Ganapathe, MA Mohamed, RM Yunus and DD Berhanuddin. Magnetite (Fe_3O_4) nanoparticles in biomedical application: From synthesis to surface functionalisation. *Magnetochemistry* 2020; **6(4)**, 68.

[20] BE Keshta, AH Gemeay, DK Sinha, S Elsharkawy, F Hassan, N Rai and C Arora. State of the art on the magnetic iron oxide nanoparticles: Synthesis, functionalization, and applications in wastewater treatment. *Results in Chemistry* 2024; **7**, 101388.

[21] K Parajuli, AK Sah and H Paudyal. Green synthesis of magnetite nanoparticles using aqueous leaves extracts of *Azadirachta indica* and its application for the removal of As(V) from water. *Green and Sustainable Chemistry* 2020; **10(4)**, 117-132.

[22] ST Aly, A Saed, A Mahmoud, M Badr, SS Garas, S Yahya and KH Hamad. Preparation of magnetite nanoparticles and their application in

the removal of methylene blue dye from wastewater. *Scientific Reports* 2024; **14**, 20100.

[23] D Wan, W Li, G Wang and X Wei. Size-controllable synthesis of Fe_3O_4 nanoparticles through oxidation-precipitation method as heterogeneous Fenton catalyst. *Journal of Materials Research* 2016; **31(17)**, 2608-2616.

[24] M Usman, A Ahmed, A Khalid, M Rafiq, M Algarni, AN Albalawi and M Hasan. Unveiling the synthesis of magnetically separable magnetite nanoparticles anchored over reduced graphene oxide for enhanced visible-light-driven photocatalytic degradation of dyes. *Diamond and Related Materials* 2024; **149**, 111575.

[25] NP Prasetya, R Prasetya, H Aldila, NA Wibowo, T Tanaka and B Purnama. Single-domain configuration tune high coercive field in Co-precipitated monazite-decorated cobalt ferrite nanoparticles. *Nano-Structures & Nano-Objects* 2024; **39**, 101301.

[26] S Dabagh, SA Haris, BK Isfahani and YN Ertas. Silver-decorated and silica-capped magnetite nanoparticles with effective antibacterial activity and reusability. *ACS Applied Bio Materials* 2023; **6(6)**, 2266-2276.

[27] RD Waldron. Infrared spectra of ferrites. *Physical Review* 1955; **99**, 1727-1735.

[28] NP Prasetya, RI Setiyani, K Kusumandari, Y Iriani, J Safani, A Taufiq and B Purnama. Cation trivalent tune of crystalline structure and magnetic properties in coprecipitated cobalt ferrite nanoparticles. *Materials Research Express* 2023; **10(3)**, 036102.

[29] BD Cullity and CD Graham. *Introduction to magnetic materials*. Wiley-IEEE Press, New Jersey, United States, 2008.

[30] D Jiles. *Introduction to magnetism and magnetic materials*. CRC Press, Boca Raton, 2015.

[31] H Ashraf, T Batool, T Anjum, A Illyas, G Li, S Naseem and S Riaz. Antifungal potential of green synthesized magnetite nanoparticles black coffee-magnetite nanoparticles against wilt infection by ameliorating enzymatic activity and gene expression in *Solanum lycopersicum* L. *Frontiers in Microbiology* 2022; **13**, 754292.

[32] SV Gudkov, DE Burmistrov, DA Serov, MB Rebezov, AA Semenova and AB Lisitsyn. Do iron oxide nanoparticles have significant antibacterial properties? *Antibiotics* 2021; **10(7)**, 884.

[33] HM Ali, K Karam, T Khan, S Wahab, S Ullah and M Sadiq. Reactive oxygen species induced oxidative damage to DNA, lipids, and proteins of antibiotic-resistant bacteria by plant-based silver nanoparticles. *3 Biotech* 2023; **13(12)**, 414.

[34] J Li, H Yang, R Gu, Y Dong, Y Cai, Q Zhao, Y Chen and M Huang. Fabrication of antibacterial Fe^{3+}-carboxymethylcellulose-polyacrylamide-Ag nanoparticles hydrogel coating for urinary catheters. *Colloids and Surfaces A: Physicochemical and Engineering Aspects* 2023; **672**, 131680.

[35] YP Yew, K Shameli, M Miyake, NBBA Khairudin, SEB Mohamad, T Naiki and KX Lee. Green biosynthesis of superparamagnetic magnetite Fe_3O_4 nanoparticles and biomedical applications in targeted anticancer drug delivery system: A review. *Arabian Journal of Chemistry* 2020; **13(1)**, 2287-2308.